Hindawi
International Journal of Photoenergy
Volume 2023, Article ID 8676430, 9 pages
https://doi.org/10.1155/2023/8676430

Research Article

Preparation of TiO_2 Grafted on Graphene and Study on their Photocatalytic Properties

Longli Lin, Lihua Shi, Simei Liu, and Jieyi He

Guangdong Polytechnic of Environment Protection Engineering, Guangdong, Foshan 528216, China

Correspondence should be addressed to Longli Lin; dgwhlin@126.com

Received 30 October 2022; Revised 16 February 2023; Accepted 6 April 2023; Published 22 August 2023

Academic Editor: Mark van Der Auweraer

TiO_2 has potential application prospects in the fields of environmental pollution control and energy conversion, while its characteristics including proneness to agglomeration and low activity affect practical applications. In view of this, P25 TiO_2 and graphene were taken as raw materials to prepare the modified TiO_2 catalyst. The modification mechanism of TiO_2 was explained by characterizing the phase composition, microscopic morphology, and functional groups and analyzing the specific surface area and particle size. Then, the photocatalytic performance of the material was explored by taking methyl orange as the target to be degraded. Results show that TiO_2 is well grafted to the laminated structure of graphene using physicochemical interactions among the introduced functional groups after modifying P25 TiO_2 and graphene. This way, the 10.00 $mg{\cdot}L^{-1}$ methyl orange solution is almost completely degraded within 12 min at a reaction rate that is 1.81 times higher than that of P25 TiO_2. Even after being used for 10 times, the performance still remains stable. The modification process is simple, and the method is reliable. Results can promote the practical application of TiO_2 photocatalytic technology.

1. Introduction

To reach the carbon peaking and carbon neutrality goals, developing new materials has become a major strategic target of the Made in China 2025 Initiative. TiO_2, as a new material that receives extensive concern, produces carriers (cavities and electrons) after being excited. The carriers may induce a slew of chemical reactions and play the catalytic action in environmental pollution control [1–5] and energy conversion [6, 7]. However, electrons and cavities are very likely to be recombined, which lowers the catalytic efficiency. TiO_2 is prone to agglomeration, which further weakens its catalytic performance, so it still cannot be used in practical applications. Graphene, also as a new material, plays a role in electron transfer [8] and is a popular material in energy storage and catalysis fields. Previous research has demonstrated that graphene can produce lots of pores on the nanosheets after modification [9]. Such special features are expected to solve the bottleneck problem in the application of TiO_2.

TiO_2 shows catalytic activity only when its carriers are captured by and reacted with graphene, which requires TiO_2 and graphene both to have special morphologies and form structurally stable compounds. To this end, numerous scholars have attempted to use many methods to prepare compounds, including the sol-gel method [10], hydrothermal treatment [11], and *in situ* synthesis [12]. However, the prepared compounds generally have poor dispersity and nonuniform particle sizes and shape, or they call for complicated processes, harsh conditions, and high costs. Therefore, these compounds cannot be scaled up, realize economic efficiency, and used in practical applications. In view of this, the research took P25 TiO_2 and graphene as raw materials to perform surface modification. Based on the physicochemical interactions among the functional groups introduced, TiO_2 is grafted on the surface of graphene, thus obtaining a modified TiO_2 catalyst. Afterwards, the catalytic activity and stability were tested, and the structure-function relationship of TiO_2 in the modification process was discussed.

2. Materials and Methods

2.1. The Main Reagents and Instruments. The experimental materials included P25 TiO_2 (Degussa, rutile/anatase ratio of 2 : 8) and graphene (preserved in diluent, Guizhou

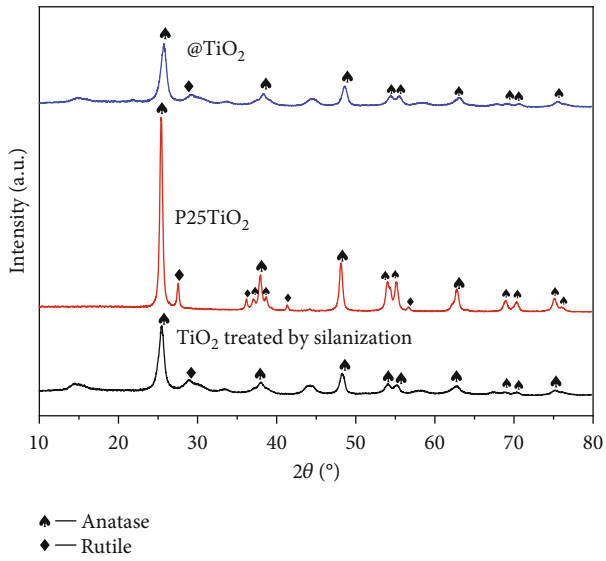

Figure 1: XRD spectra of different types TiO_2.

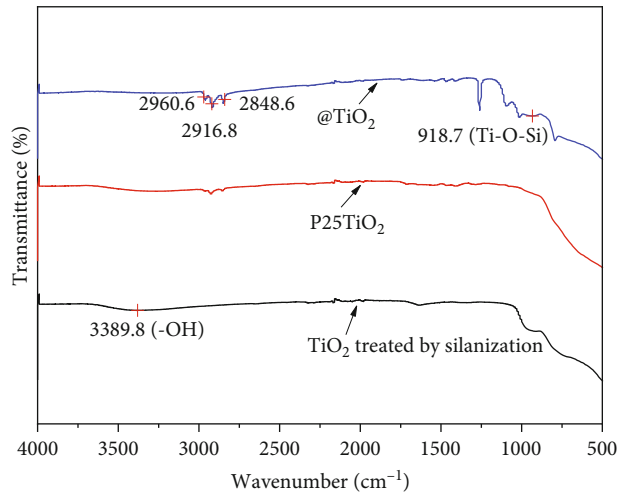

Figure 2: FTIR spectra of different types TiO_2.

Zhongshi Graphene Materials). The instruments used in the experiments included a hydrothermal reactor, a photochemical reaction apparatus [13], a 300 W mercury lamp (dominant wavelength of 365 nm, Shanghai Bilon Instrument Manufacturing Co., Ltd.), a freezer dryer (Shanghai Bilon Instrument Manufacturing Co., Ltd., BILON-FD50AE), an electric vacuum drying oven (Taizhou Yongjing Machinery Manufacturing Co., Ltd., DZ-1AII), a heat-collecting constant-temperature heating magnetic stirrer (Shanghai Lichen-Bx Instrument Technology Co., Ltd., DF-101), and a centrifugal separator (Jiangsu Tianli Medical Devices Co., Ltd., TL80-1). Reagents including methyl orange (Aladdin®), γ-aminopropyl triethoxysilane as the coupling agent (KH-550), and hydrazine hydrate were all analytically pure.

Catalysts were characterized and identified by means of attenuated total reflectance Fourier-transform infrared spectroscopy (ATR-FTIR, Thermo Scientific Nicolet iS50), X-ray diffraction (XRD, Bruker D8 Advance), full automatic specific surface and aperture analyzer (Micromeritics ASAP2460), and scanning electron microscopy (SEM, Coxem Oxford, EM-30 N).

2.2. Preparation of Modified TiO_2

2.2.1. P25 TiO_2 Modification. The raw material P25 TiO_2 was subjected to hydrothermal synthesis [2] and then preserved for later use and testing. A certain amount of treated P25 TiO_2 was weighed and experienced silanization [13], washing, filtration, and vacuum drying successively to obtain samples (marked as @TiO_2), which were preserved for later use and testing.

2.2.2. Graphene Modification. A certain amount of graphene diluent was weighed at first, then washed, filtrated, and freeze-dried to obtain granular graphene (marked as GR), which was uniformly dispersed in a mixed solution of concentrated sulfuric acid and concentrated nitric acid with a matching ratio of 1 : 1 ($v \cdot v^{-1}$). Then, a certain amount of potassium permanganate was added in the solution to allow the reaction for 1 h. Afterwards, the products were treated via ultrasound, washed, filtrated, and freeze-dried for later use. A certain amount of the products was weighed, in which slight hydrazine hydrate was added to react for 30 min. The sample obtained after washing, filtration, and freeze-drying was termed as RGO, which was preserved for later use and testing.

2.2.3. Preparation of Modified TiO_2. Certain amounts of P25 TiO_2, @TiO_2, and RGO were weighed, mixed according to a ratio of 1 : 1 ($m \cdot m^{-1}$), and then sufficiently ground in an agate mortar. The resulting products were parceled with a tinfoil and kept in the dark for 24 h, thus preparing the modified TiO_2 (marked as @TiO_2/RGO). The composite samples of P25 TiO_2 and RGO (marked as P25 TiO_2/RGO) were preserved for later use and testing.

2.3. Photocatalytic Experiment. The photocatalytic activity and stability of modified TiO_2 were characterized by taking 10.00 $mg \cdot L^{-1}$ methyl orange (initial pH, 7.80 ± 0.2) as the target to be degraded. Under a 300 W high-pressure mercury lamp (the average light intensity in solutions was about 8 MW/cm^2) which served as a light source and a catalyst dosage of 5 $g \cdot L^{-1}$, the reaction was performed in a stirring reactor [13]. The temperature of the reactor was regulated at 26 ± 0.5 °C by a circulating water system. After 12 min irradiation, the final pH values of samples were determined. The concentration of methyl orange was analyzed by using a 722 visible light spectrophotometer in a cuvette with the thickness of 1 cm at the wavelength of 465 nm. The degradation efficiency for methyl orange can be calculated by the following equation:

$$\eta = \frac{c_0 - c_t}{c_0} \times 100\%, \quad (1)$$

where η is moment degradation efficiency, C_0 and C_t are the initial concentration and the moment concentration of methyl orange in mg/L, respectively.

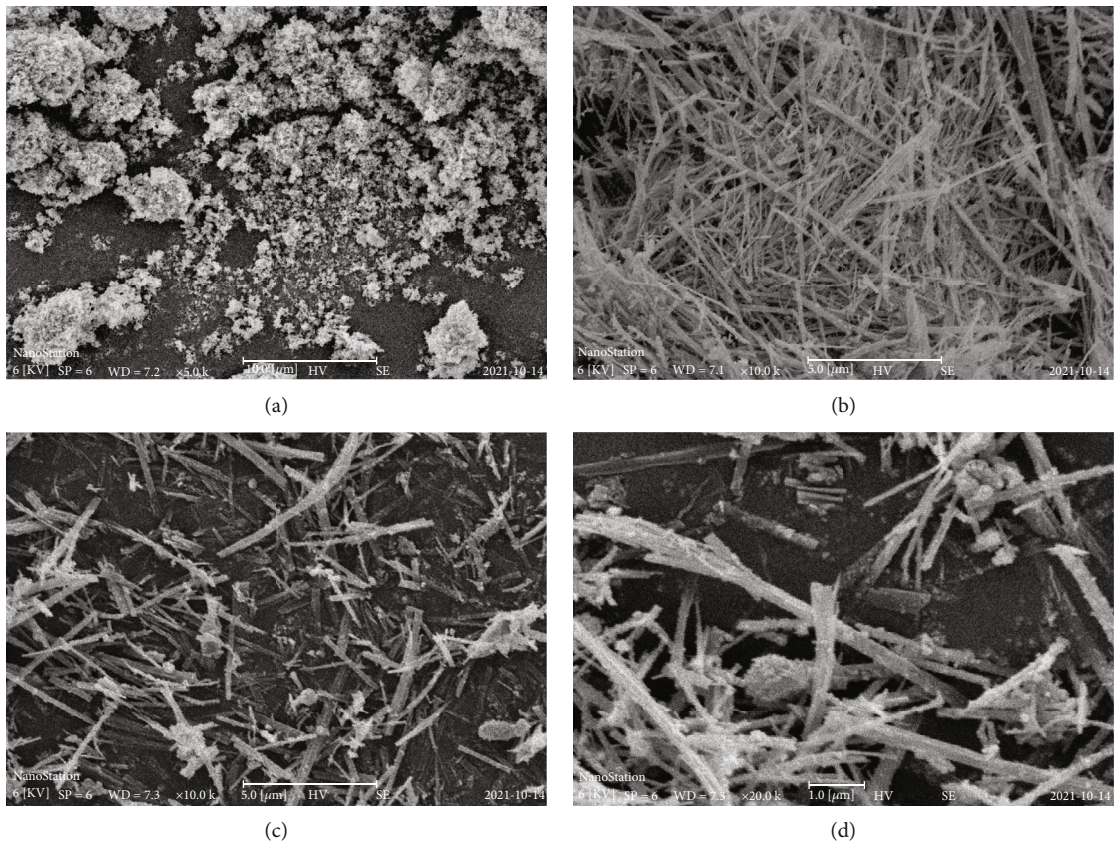

Figure 3: SEM images of P25 TiO_2 (a), TiO_2 prepared through hydrothermal synthesis (b), and @TiO_2 (c, d).

Table 1: Specific surface areas and particle sizes of different types TiO_2.

Sample	Specific surface areas($m^2 \cdot g^{-1}$)	Particle sizes(nm)
P25TiO_2	48.2[1]	21[1]
@TiO_2	63.4	94

[1]Data from https://b2b.baidu.com/land?id=7461b39899af70cf609dc7e48498ab5610.

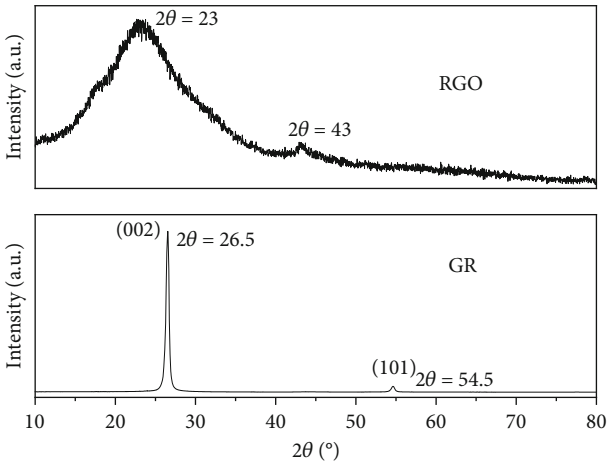

Figure 4: XRD spectra of GR and RGO.

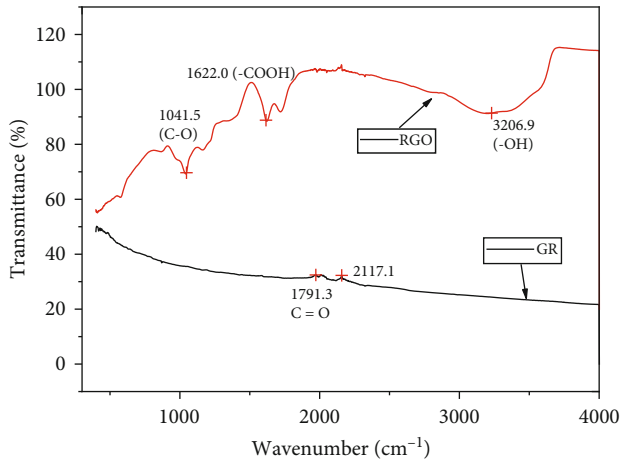

Figure 5: FTIR spectra of GR and RGO.

3. Results and Analysis

3.1. Characterization of TiO_2. P25 TiO_2 and @TiO_2 were characterized through XRD, FTIR, and scanning electron microscopy (SEM). Their specific surface areas and particle sizes were analyzed. The results are shown in Figures 1–3 and Table 1. Figure 1 shows that P25 TiO_2 is a mixed crystal of anatase and rutile. Through hydrothermal synthesis (high-temperature and high-pressure reaction), a small amount of rutile is transformed into

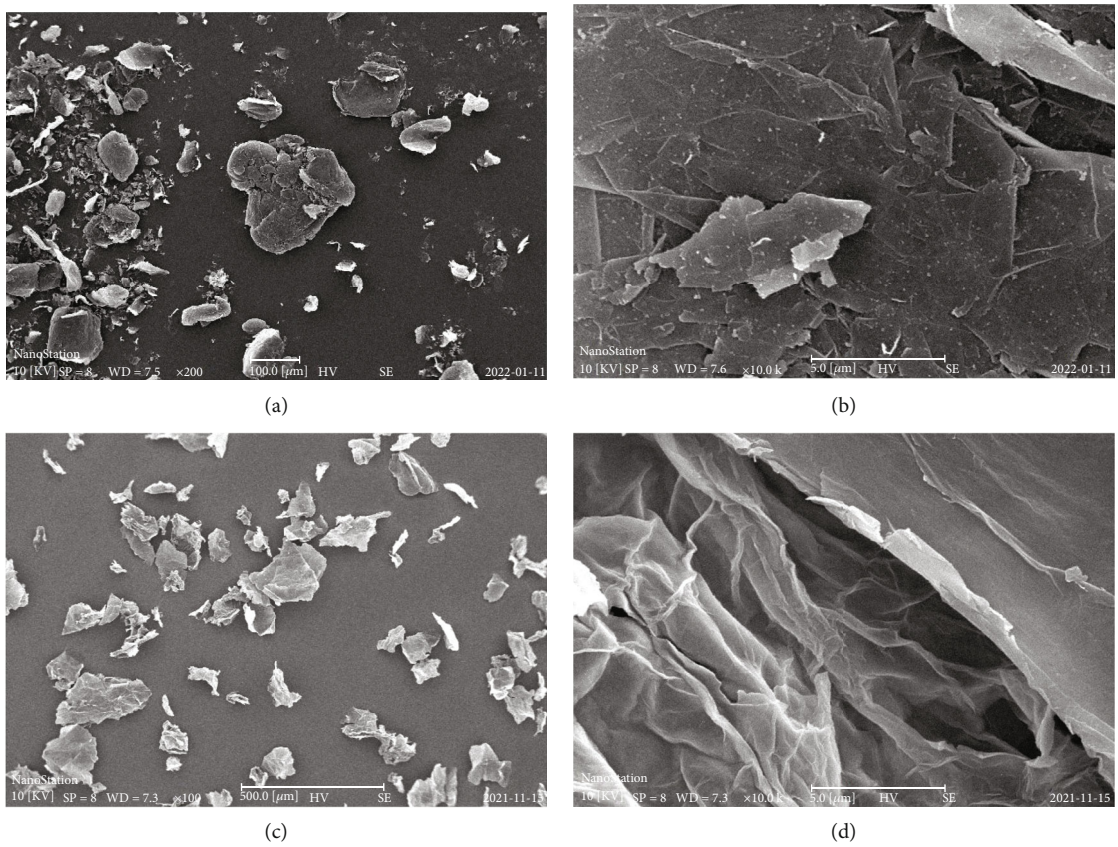

Figure 6: SEM images of GR (a, b) and RGO (c, d).

Table 2: Specific surface areas and pore size distribution of GR and RGO.

Sample	Specific surface areas ($m^2 \cdot g^{-1}$)	Macropores (content%)	Mesopores (content%)	Micropores (content%)
GR	163.0	50-172 nm(45.27)	2-31 nm(54.62)	<2 nm(0.11)
RGO	236.7	80-207 nm(47.01)	2-47 nm(47.37)	<2 nm(5.62)

anatase. Previous research demonstrates that the transformation is conducive to the improvement of the activity [14]. In comparison, the silanization does not significantly influence the crystal form of TiO_2 but still remains the mixed crystal structure. As shown in Figure 2, P25 TiO_2 does not have any absorption peak, while a strong absorption peak appears at 3389.9 cm^{-1} after hydrothermal synthesis, which is a stretching vibration peak of O-H. This indicates that hydroxyl groups are introduced on the TiO_2 surface after hydrothermal synthesis. For @TiO_2, an absorption peak of Ti-O-Si appears at 918.7 cm^{-1} [15], suggesting the presence of a condensation reaction between silanol (the hydrolysis product of the silane coupling agent) and hydroxyl groups on the TiO_2 surface. This way, aminopropyl siloxane containing amidogen groups is introduced to the surface of TiO_2. Because amidogen groups carry positive charges, the modified TiO_2 is positively charged [16]. Peaks at 2848.6, 2916.8, and 2960.6 cm^{-1} are stretching vibration peaks of methene ($-CH_2$). It can be seen in Figure 3(a) that P25 TiO_2 is nonuniformly distributed and agglomerated; Figure 3(b) depicts that TiO_2 prepared through hydrothermal synthesis is an acicular crystal, which is then coarsened and becomes rod-like or tubular after silanization, with protuberant ends. This is probably because aminopropyl siloxane containing amidogen groups is grafted on the TiO_2 surface, as displayed in Figures 3(c) and 3(d). According to Table 1, P25 TiO_2 is transformed from a granular state with the average particle size of 21 nm to rod-like or tubular @TiO_2 with the particle size of 20~200 nm and length of 1~4 μm. Under the condition, the specific surface area of TiO_2 enlarges by 31.5%, and TiO_2 becomes less prone to agglomeration. Theoretically, these phenomena are all favorable for improving the catalytic performance.

3.2. Characterization of Graphene. GR and RGO were characterized through XRD, FTIR, and SEM. Their specific surface areas and pore sizes were analyzed. The results are displayed in Figures 4–6 and Table 2. It can be seen in Figure 4 that compared with GR, RGO has a higher and unstable baseline with widened peaks, which is probably because the substitution effect of oxygen atoms is introduced

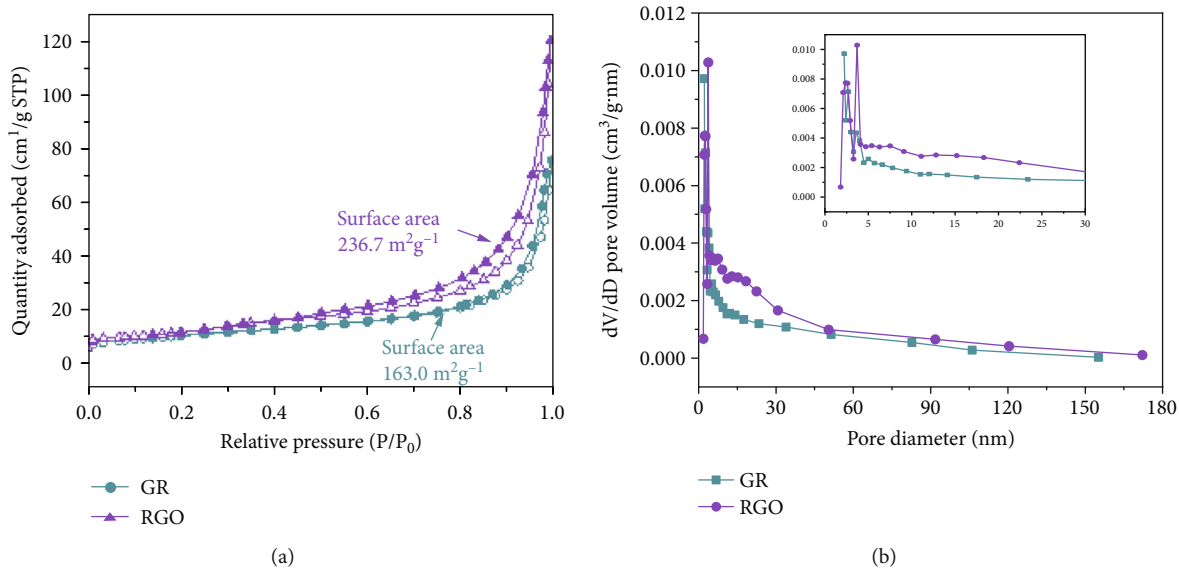

Figure 7: (a) The GR and RGO adsorption/desorption isotherms. (b) The curves illustrating the pore size distribution of GR and RGO.

due to oxidation. As a result, the carbon atoms combined with the oxygen atoms differ from other carbon atoms. Such a difference impairs the original stress equilibrium of carbon atoms, causes lattice distortion, and forms lattice defects, thus leading to widened and weakened diffraction peaks. Formation of defects is favorable for improving the electron transfer capacity of graphene [8]. Graphene is usually stored in the diluent, which mainly contains pennyroyal tea and castor leaf. After washing before usage, there are still probably some residual impurities. Therefore, it can be seen in Figure 5 that the peak at 1791.3 cm^{-1} is a stretching vibration peak of C=O in the molecular structures of pennyroyal tea and castor leaf; the peak at 2117.1 cm^{-1} is probably ascribed to the residual impurities; these peaks all disappear after oxidation. Oxygen-containing groups such as hydroxyl and carboxy groups are interpenetrated on the surface of RGO. Owing to the presence of these functional groups, the RGO surface is negatively charged [16]. As displayed in Figures 6(a) and 6(b), GR is indeed agglomerated, while tightly bonded laminated structures are also observed, with small pores distributed on the surface. According to Table 2, the pore size is distributed in the range of 2~31 nm, which mainly are mesopores that are formed due to the accumulation of particles. As shown in Figures 6(c) and 6(d), the modification did not destroy the lamellar structure of GR which is more seriously stripped; leading to the laminated structure becomes increasingly obvious. Sheet-like lamellas become larger, thinner, and transparent, without agglomeration.

As shown in Figure 7(a) and Table 2, the modification changes the specific surface area, pore volume, and structure of the material, making RGO and GR present obvious differences. It may be due to the difference between carbon atoms combined with oxygen and other carbon atoms, stress nonequilibrium occurs, and several irregularly distributed folds are formed on the surface. It can be clearly seen in Figure 6(d) that new channels are formed by these folds, which is the main cause for the gradual increase in the number of macropores and micropores in the modification process of graphene. However, as shown in Figure 7(b) and Table 2, the total number of micropores is still small and the channels are mainly composed of macropores and mesopores that are formed because of the accumulation of lamellas. The pore sizes are mainly in the ranges of 2~47 nm and 80~207 nm, and the specific surface area enlarges by 45.2%. Theoretically, all these changes are conducive to the improvement of the properties of graphene.

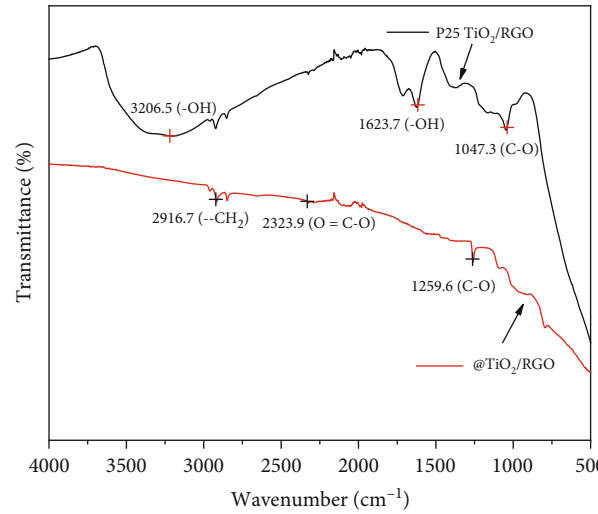

Figure 8: Comparison of FTIR spectra of P25 TiO$_2$/RGO and @TiO$_2$/RGO.

3.3. Characterization of Composite Materials. Two composite samples, P25TiO$_2$/RGO and @TiO$_2$/RGO, were characterized through FTIR and SEM, and the results are displayed in Figures 8 and 9. It can be seen in Figure 8 that the absorption peaks of the composite sample of P25TiO$_2$ and RGO at 3206.5, 1623.7, and 1047.3 cm^{-1} are

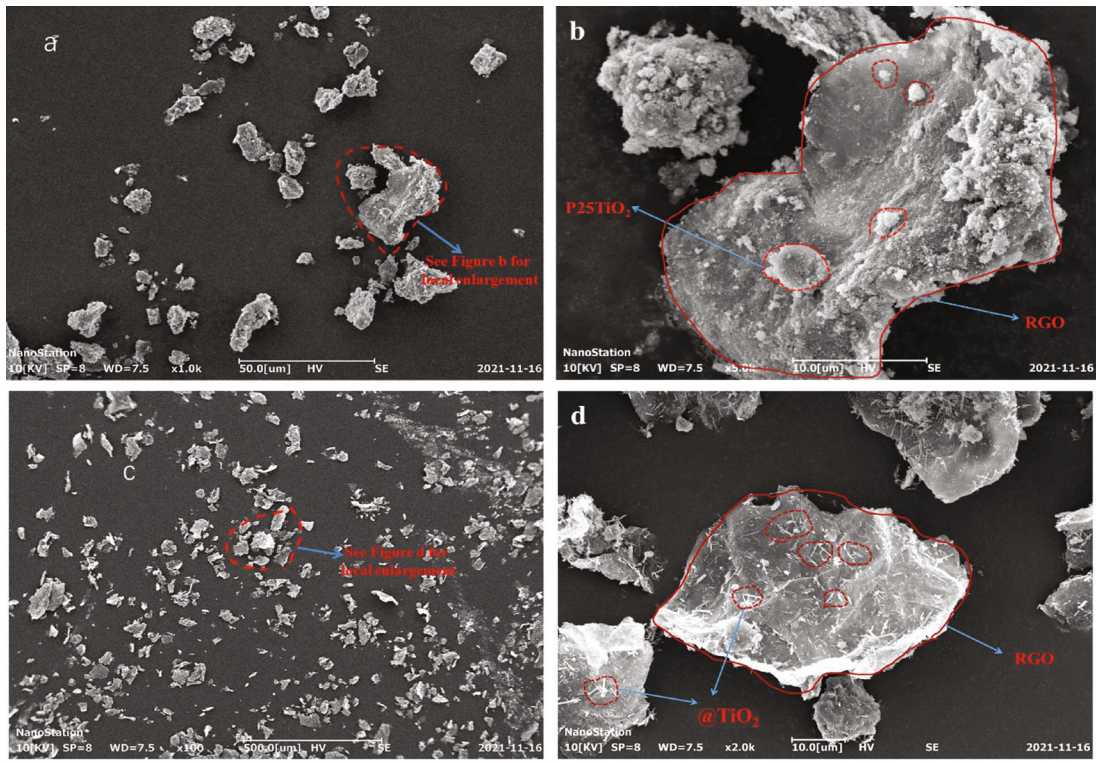

Figure 9: (a) SEM image of P25TiO_2/RGO. (b) The locally enlarged image of (a). (c) SEM image of @TiO_2/RGO. (d) The locally enlarged image of (c).

Table 3: The initial pH and the final pH values of samples.

The initial pH values	The final pH values
7.80	8.41

very approximated to those of RGO in Figure 5 (3206.9, 1622.0, and 1041.5 cm^{-1}). No new absorption peaks appear, which means that no physicochemical interactions occur even if P25 TiO_2 is mixed with RGO that contains abundant oxygen-containing groups, as evinced by the agglomeration and non-uniform distribution in Figure 9(a). Figure 9(b) shows that TiO_2 particles are simply accumulated on the surface of RGO. When @TiO_2 and RGO are mixed, a new peak appears at 2323.9 cm^{-1}, which belongs to the absorption peak of ester groups, indicative of the condensation reaction between RGO and TiO_2. According to the analysis in Section 3.2, lots of negatively charged oxygen-containing groups are interpenetrated on the surface of RGO. As mentioned in Section 3.1, amidogen groups with positive charges are introduced on the @TiO_2 surface. The two also have electrostatic attraction. Therefore, TiO_2 is grafted on the laminated structure of RGO under the dual effects of electrostatic attraction and condensation reaction, thus obtaining the modified TiO_2. It can be seen in Figure 9(c) that the sample is uniformly distributed and not agglomerated. As illustrated in Figure 9(d), rod-like or tubular TiO_2 is uniformly distributed on the surface of RGO.

3.4. Effect of Solution pH on the Degradation Kinetics. The initial and final pH values of samples were summarized as displayed in Table 3. The results show that the pH of the system will increase with the photodegradation process of methyl orange. As a result, the system's alkalinity will gradually be increased. Such a phenomenon can be attributed to hydrogen generation by the following reaction:

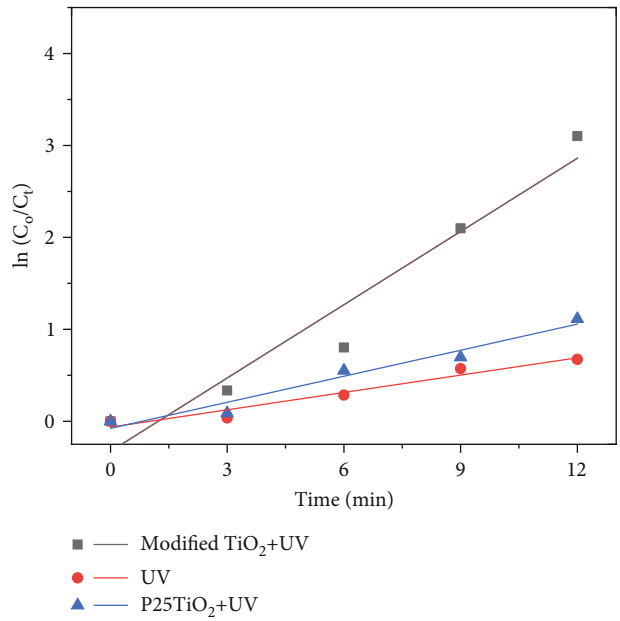

Figure 10: Changes in degradation of methyl orange with time under different conditions.

$$2H^+ + 2e^- \longrightarrow H_2, \quad (2)$$

Table 4: Kinetic results of methyl orange degradation by TiO_2 photocatalysis.

Sample	k [a]/min^{-1})	Half-life($t_{1/2}$/min)	RSQ[b]	Removal efficiency in 12 min (%)
UV	0.06286	11.03	0.951	49.05
P25T iO_2+UV	0.09443	7.34	0.961	67.14
Modified TiO_2+UV	0.2655	2.62	0.941	95.50

k[a] is the first-order kinetic constant obtained using $\ln(C_0/C_t) = kt$, RSQ[b] = R-squared.

indicating that H^+ would be reduced by electrons which may be transferred from TiO_2 to graphene surface. The hydrogen ions are mainly generated from the hydrolysis of methyl orange which will be inhibited by the rise of pH.

Moreover, the increase of pH will affect the forms and adsorption of ionizable compounds [17]. Specifically, it also greatly influences the surface properties of the catalyst, which can be described through Equation (3), showing that pH will affect the redox ability of the photocatalyst

$$E_{VB}(V) = +2.9 - 0.059pH. \quad (3)$$

Apparently, the increase of solution pH was not conducive for the removal of methyl orange.

3.5. Photocatalytic Performance of Modified TiO_2. To characterize the catalytic activity of modified TiO_2 (@TiO_2/RGO), the photocatalytic degradation experiments on methyl orange were conducted following the steps in Section 2.3 taking P25TiO_2(P25TiO_2/RGO) as the control. Because the reaction at a low concentration is approximated to the first-order catalytic reaction [(2)], $\ln(C_0/C_t)$ was used to draw plots about the reaction time (Figure 10). Kinetic parameters are calculated according to the first-order reaction, as listed in Table 4. It shows that the degradation rate of methyl orange by modified TiO_2 is 1.81 times, 0.52 times higher than that by P25 TiO_2 and immobilized PU/TiO_2 [18], respectively. The removal efficiency of methyl orange by modified TiO_2 within 12 min is also improved by 0.42 times, suggesting the better catalytic activity of modified TiO_2.

In general, catalytic activity will be declined when the catalyst is repeatedly used. In response to this situation, the photocatalytic stability was investigated. Experiments on photocatalytic degradation of methyl orange were carried out for ten times repeatedly. Then, the catalyst was centrifugalized and freeze-dried. It was weighted to be 0.0786 g. Changes in the removal efficiency with the times of repetition are shown in Figure 11. As shown in the figure, the degradation efficiency of methyl orange reduces slightly after each use, while the reduction of removal efficiency is closely correlated with the loss of catalyst ($R^2 = 0.998$). This indicates that the reduction of catalytic efficiency results from the loss of the catalyst, rather than the falling off and inactivation of the catalyst, which indicates the high stability of the modified TiO_2.

As mentioned in Section 3.4, increasing pH is unconducive to the photocatalytic degradation of methyl orange. However, the composite catalyst still exhibits good catalytic activity. As shown in Figures 9(c) and 9(d), a complex with intimate interface was obtained by integrating graphene with TiO_2, which invests the sample with prominent photocatalytic abilities. Such a phenomenon can be explained by the fact that the modification imparts better catalytic performance to the material (for example, the introduced hydroxyl groups also have catalytic activity, enlarged specific surface area, and are not easily agglomerated, as shown in Section 3.1). Apart from this, graphene itself is characterized by π-π stacking, which provides stronger adsorption advantages for materials containing benzene rings such as methyl orange [1]. And adsorption is the primary condition for the occurrence of catalytic reactions [13].

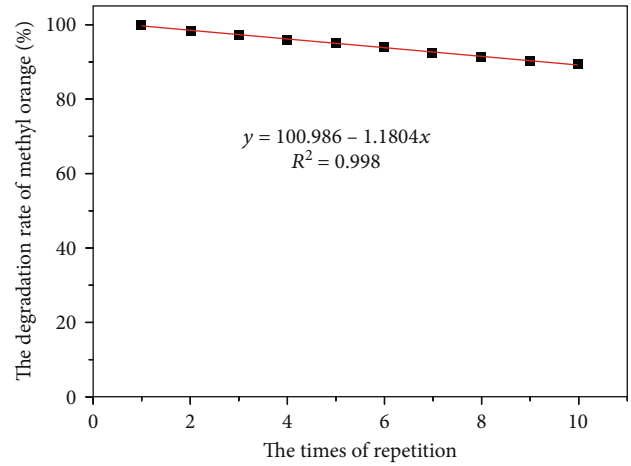

Figure 11: Changes in the degradation efficiency of methyl orange by modified TiO_2 with the times of repetition.

Moreover, graphene itself has excellent mechanical, thermal, optical, and electrical properties, and its performance is further optimized after modification: (1) it has a larger specific surface and better dispersity, which avoids TiO_2 shield effective absorption of photons due to proneness to agglomeration and enlarges the contact interface between graphene and TiO_2, as shown in Section 3.2. (2) Graphene alters the energy band structure of TiO_2 in the complex, reducing the band gap width from 3.20 eV to 2.64 eV [19]. Similarly, graphene in the compound can change the energy band structure of TiO_2, which has been verified in N-TiO_2/graphene, decreasing the width from 2.92 eV to 2.73 eV [20]. With the decrease in the band gap energy of TiO_2, more photogenerated electrons reach their escape work and then are transferred to graphene surface via the composite interface [8, 21]. Mott-Schottky diagram and DOS images can verify the increment in density of carriers [22, 23]. 3) As can be seen in Section 3.2, there are abundant narrow holes distributed on graphene surface. This is because modification can introduce oxygen atoms into graphene, inducing the graphene to generate lattice defects. As a consequence,

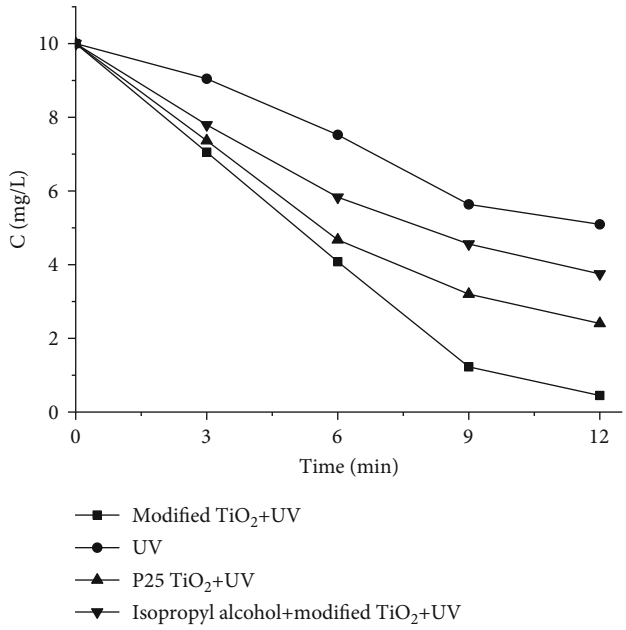

Figure 12: Comparison of photocatalytic degradation of methyl orange with and without isopropanol.

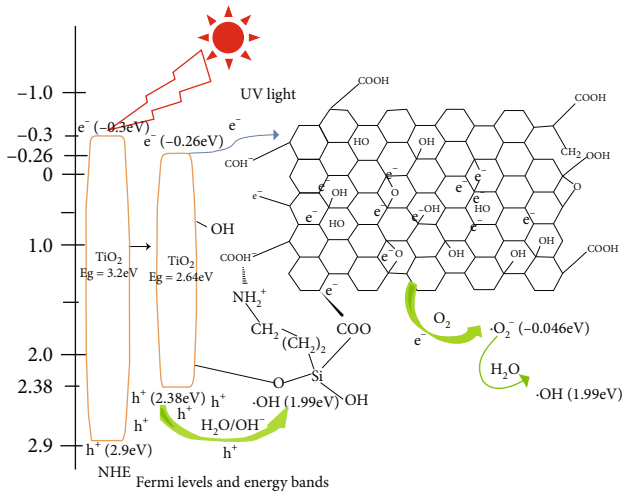

Figure 13: Schematic diagram of TiO_2 photocatalytic performance improvement mechanism.

multichannel structures were formed on graphene surface, which change [24] and shorten [25] the transfer paths of charges and speed up the charge transfer rate.

In summary, multiple factors collaboratively promote interfacial charge separation. The reaction as shown in Equation (2) occurs to partial electrons transferred, while some electrons are subject to the reaction as presented in Equation (4), for the more holes remained, which are mainly consumed through Equation (5). Equations (2), (4), and (5) are beneficial to inhibit the recombination of electron-hole pairs. This makes the photocarriers to generate more active species [22].

$$e^- + O_2 \longrightarrow \cdot O_2^- \quad \cdot O_2^- + H_2O \longrightarrow \cdot OH, \tag{4}$$

$$h^+ + OH^-(H_2O)_{abs} \longrightarrow \cdot OH. \tag{5}$$

Bell et al. [26] consider that these active substances, mainly $\cdot O_2^-$ and ·OH, have high activity, significantly improving the photocatalytic activity of the composite catalyst. In order to identify the active oxidation species, the quenching experiment of isopropyl alcohol was conducted [27] (eliminating hydroxyl radical), as shown in Figure 12. The results showed that modified TiO_2 produced a large amount of ·OH under ultraviolet light. In summary, as discussed above, various factors synergize to reinforce the catalytic activity of TiO_2. The improvement mechanism of the catalytic performance is illustrated in Figure 13.

4. Conclusions

In a nutshell, it can be concluded that (1) by modifying P25 TiO_2, hydroxyl, and amidogen groups are successively introduced to the surface, and the material turns from a granular one to a rod-like or tubular one, with a small amount of rutile transformed into anatase. After modifying graphene, oxygen-containing groups are introduced to the surface, and the laminated structure is stripped off sufficiently. At the same time, lattice defects appear, and new multichannel structures are formed. Through physicochemical interactions, TiO_2 is grafted on the laminated structure of graphene, thus obtaining the modified TiO_2 catalyst. (2) The modified TiO_2 is able to almost completely degrade the 10.00 mg·L^{-1} methyl orange solution within 12 min. The reaction rate is improved by 1.81 times compared with P25 TiO_2, and the catalytic performance still remains stable even after repetitious usage. This solves the problems of proneness to agglomeration and low activity of TiO_2 in practical applications effectively.

Data Availability

Data are available on request from the authors. The raw/processed data for these findings cannot be shared at this time as the data are also part of an ongoing study.

Conflicts of Interest

The authors declare that they have no conflicts of interest.

Acknowledgments

This work was supported by the Innovation Projects of Colleges in Guangdong Province (2021KTSCX252 and 2022WTSCX219) and the Dean's fund project of Guangdong Polytechnic of Environment Protection Engineering (K650121042304).

References

[1] Z. Shenping, W. Yimeng, Y. Ge, H. Jun, and L. Honglai, "Degradation of antibiotics by porous composite photocatalyst," *Chemical Industry and Engineering Progress*, vol. 40, no. 6, pp. 3287–3299, 2021.

[2] L. L. Lin, M. J. Yang, Y. Zhang, Z. P. Liu, S. H. Chen, and M. J. Zhang, "Photocatalytic removal of chelated silver by TiO_2 nanotube synergetic mechanism between Ag(I) and organic ligands," *Chinese Journal of Environmental Engineering*, vol. 10, no. 2, pp. 704–708, 2016.

[3] Z. S. Wang and H. S. Li, "Degradation of pigment production wastewater via a K2S2O8-doped TiO_2 photocatalyst," *Industrial Water Treatment*, vol. 40, no. 2, pp. 55–58, 2020.

[4] S. Saleh, S. Mohammadnejad, H. Khorgooei, and M. Otadi, "Photooxidation/adsorption of arsenic (III) in aqueous solution over bentonite/ chitosan/TiO_2 heterostructured catalyst," *Chemosphere*, vol. 280, article 130583, 2021.

[5] P. Alulema-Pullupaxi, F. Lenys, D. Alexis et al., "Photoelectrocatalytic degradation of glyphosate on titanium dioxide synthesized by sol-gel/spin-coating on boron doped diamond (TiO_2/BDD) as a photoanode," *Chemosphere*, vol. 278, article 130488, 2021.

[6] X. Zhang, Z. Leng, M. Gao et al., "Enhanced hydrogen storage properties of MgH_2 catalyzed with carbon-supported nanocrystalline TiO_2," *Journal of Power Sources*, vol. 398, no. 15, pp. 183–192, 2018.

[7] G. S. Zhang, *TiO_2 and Graphene/Ni(OH)$_2$ Electrode Materials for Energy Storge*, University of Technology, Dalian, China, 2013.

[8] I. V. Lightcap, T. H. Kosel, and P. V. Kamat, "Anchoring semiconductor and metal nanoparticles on a two-dimensional catalyst mat. Storing and shuttling electrons with reduced graphene oxide," *Nano Letters*, vol. 10, no. 2, pp. 577–583, 2010.

[9] S. J. Wan, X. Li, Y. Chen et al., "High-strength scalable MXene films through bridging-induced densification," *Science*, vol. 374, no. 6563, pp. 96–99, 2021.

[10] C. Chen, Z. Chen, and X. Zen, "Synthesis of grapheme oxide/titanium dioxide composite material by thermal reduction method and its photocatalytic acivity," *Journal of Functional Materials*, vol. 46, no. 16, pp. 16152–16156, 2015.

[11] F. Y. Pei, S. G. Xu, Y. L. Liu et al., "Photocatalytic hydrogen evolution from water by dye-sensitized titania/graphene nanocomposite," *CIESC Journal*, vol. 64, no. 8, pp. 3062–3069, 2013.

[12] Y. Liang, H. Wang, H. S. Casalongue, C. Zhuo, and H. Dai, "TiO_2 nanocrystals grown on graphene as advanced photocatalytic hybrid materials," *Nano Research*, vol. 3, no. 10, pp. 701–705, 2010.

[13] L. L. Lin, G. G. Liu, M. J. Yang, Y. Zhang, and H. M. Ji, "Preparation and photocatalytic properties of TiO_2 nanotubes supported on polyurethane membrane," *Materials Review*, vol. 29, no. 8, pp. 149–153, 2015.

[14] W. Gao, F. Q. Wu, Z. Luo, J. X. Fu, and B. K. Xu, "Studies on the relationship between the crystal form of TiO_2 and its photocatalyzing degradation efficiency," *Chemical Journal of Chinese Universities*, vol. 22, no. 4, pp. 660–662, 2001.

[15] Z. Li, H. Bo, Y. Xu et al., "Comparative study of sol-gel-hydrothermal and sol-gel synthesis of titania- silica composite nanoparticles," *Journal of Solid State Chemistry*, vol. 178, no. 5, pp. 1395–1405, 2005.

[16] J. S. Lee, K. H. You, and B. P. Chan, "Highly photoactive, low bandgap TiO_2 nanoparticles wrapped by graphene," *Advanced Materials*, vol. 24, no. 8, pp. 1084–1088, 2012.

[17] Z. L. Lin, Y. L. Wu, X. Y. Jin et al., "Facile synthesis of direct Z-scheme UiO-66-NH_2/PhC_2Cu heterojunction with ultrahigh redox potential for enhanced photocatalytic Cr(VI) reduction and NOR degradation," *Journal of Hazardous Materials*, vol. 443, article 130195, 2023.

[18] L. L. Lin, Q. J. Wu, X. Gong, and Y. Zhang, "Preparation of TiO_2 nanotubes loaded on polyurethane membrane and research on their photocatalytic properties," *Journal of Analytical Methods in Chemistry*, vol. 2017, Article ID 9629532, 6 pages, 2017.

[19] D. M. Jia, X. Y. Li, Q. Q. Chi et al., "Direct electron transfer from upconversion graphene quantum dots to TiO2enabling infrared light-driven overall water splitting," *Research*, vol. 2022, article 9781453, 9 pages, 2022.

[20] W. F. Zhao, J. L. Duan, B. Ji, L. Z. Ma, and Z. Yang, "Novel formation of large area N-TiO_2/graphene layered materials and enhanced photocatalytic degradation of antibiotics," *Journal of Environmental Chemical Engineering*, vol. 8, no. 1, article 102206, 2020.

[21] P. V. Kamat, "Graphene-based nanoarchitectures. Anchoring semiconductor and metal nanoparticles on a two-dimensional carbon support," *Journal of Physical Chemistry Letters*, vol. 1, no. 2, pp. 520–527, 2010.

[22] S. J. Li, M. J. Cai, Y. P. Liu et al., "In situconstruction of a C3N5nanosheet/Bi2WO6nanodot S-scheme heterojunction with enhanced structural defects for the efficient photocatalytic removal of tetracycline and Cr(VI)," *Inorganic Chemistry Frontiers*, vol. 9, no. 11, pp. 2479–2497, 2022.

[23] D. Xu, S. N. Zhang, J. S. Chen, and X. H. Li, "Design of the synergistic rectifying interfaces in Mott–Schottky catalysts," *Chemical Reviews*, vol. 123, no. 1, pp. 1–30, 2023.

[24] Y. Su, Z. Zhang, H. Liu, and Y. Wang, "$Cd_{0.2}Zn_{0.8}S$@UiO-66-NH_2 nanocomposites as efficient and stable visible-light-driven photocatalyst for H_2 evolution and CO_2 reduction," *Applied Catalysis B: Environmental*, vol. 200, pp. 448–457, 2017.

[25] H. Liu, J. Zhang, and D. Ao, "Construction of heterostructured $ZnIn_2S_4$@NH_2-MIL-125(Ti) nanocomposites for visible-light-driven H_2 production," *Applied Catalysis B: Environmental*, vol. 221, pp. 433–442, 2018.

[26] N. J. Bell, Y. H. Ng, D. Aijun, H. Coster, S. C. Smith, and R. Amal, "Understanding the enhancement in photoelectrochemical properties of photocatalytically prepared TiO_2-reduced graphene oxide composite," *Journal of Physical Chemistry C*, vol. 115, no. 13, pp. 6004–6009, 2011.

[27] G. V. Buxton, C. L. Greenstock, W. Phillips Helman, and A. B. Ross, "Critical review of rate constants for reactions of hydrated electrons, hydrogen atoms and hydroxyl radicals(·OH/·O^- in aqueous solution)," *Journal of Physical and Chemical Reference Data*, vol. 17, no. 2, pp. 513–886, 1988.